A Detailed Theoretical Treatment of the Partial Oxidation of Methane to Syngas on Transition and Coinage Metal (M) Catalysts (M = Ni, Pd, Pt, Cu)

Chak-Tong Au,[†] Meng-Sheng Liao,*[,†,‡] and Ching-Fai Ng[†]

Department of Chemistry, Hong Kong Baptist University, Kowloon, Hong Kong, and Department of Chemistry, Xiamen University, Xiamen 361005, People's Republic of China

Received: September 15, 1997; In Final Form: February 17, 1998

This paper presents a detailed theoretical treatment of the partial oxidation of methane to syngas (OMS) on transition and coinage metal (M) catalysts (M = Ni, Pd, Pt, Cu). The adsorption energies for a number of intermediates in the dissociation of methane on the metals were calculated using medium sized cluster models of 7−13 atoms. Reaction energies for methane dissociation, syngas formation, and byproduct generation were determined. The activation energies were estimated by means of the analytic BOC-MP formula. On the basis of these results, several significant aspects involved in the OMS on the metal catalysts have been elucidated. (1) The total dissociation energy (D_e) for the complete dissociation of methane to give surface carbon and hydrogen ($CH_{4,s} \rightarrow C_s + 4H_s$) can be regarded as a measure for the activity of the metal in methane dissociation. The order of the calculated D_e's is consistent with the order of methane conversions over the metals. (2) In the presence of coadsorbed oxygen, oxygen at metal on-top site increases the adsorption energy of H and promotes methane dehydrogenation. Oxygen at the hollow site may or may not promote methane dehydrogenation, depending on the metal. (3) For the possible reactions for the coupling of the intermediates on the metal surfaces, $CH_{x,s} + CH_{x,s} \rightarrow C_2H_{2x,s}$, the trend in the calculated combination energies is in agreement with experimental observation.

1. Introduction

In recent years, there has been increased interest in the catalytic selective partial oxidation of methane to syngas (OMS):

$$CH_4 + {}^1/_2O_2 \rightarrow CO + 2H_2 \qquad (1)$$

In contrast to the methane steam reforming ($CH_4 + H_2O \rightarrow CO + 3H_2$) reaction, this process is mildly exothermic and produces a desired H_2/CO ratio. The reaction proceeding over a nickel catalyst was studied by Prettre et al.[1] Very recently, a series of supported nickel and noble metal catalysts (Rh, Ru, Ir, Pd, Pt) was found to perform well in terms of methane conversion and syngas selectivity.[2−13] Two different reaction schemes have been proposed in the literature. As early as 1946, Prettre et al.[1] postulated that the reaction pathway involves the initial conversion of a fraction of the methane feed to CO_2 and H_2O, followed by the steam reforming, CO_2 reforming, and water−gas shift reactions. This opinion was accepted by a number of recent researchers.[2−4] The other scheme is direct oxidation via methane pyrolysis as proposed by Schmidt et al.[5,6] on the basis of experiments over monolith-supported Rh and Pt catalysts at short contact time. According to these authors, the dissociation of methane was an initial step for CO and H_2 productions, and CO_2 was the secondary product of CO oxidation. The direct conversion of methane to syngas was also reported by Choudhary's group,[7] who employed catalysts containing nickel and cobalt, and operated the CH_4 oxidation reaction at extremely high space velocities. Later, a number of pulse studies[8−13] of the partial oxidation of methane over catalysts containing nickel, rhodium, and platinum were performed. A temporal analysis of the products indicated a direct oxidation initiated by methane dissociation, which results in the formation of surface carbon and hydrogen. Different mechanisms have been proposed for the formation of CO on reduced metals.[5−13] Some authors[8−10] suggested that CO_2 is formed as a primary product and that the formation of CO proceeds via a fast reaction of carbon species with CO_2. Others[5,6,11,12] concluded that methane oxidation to syngas occurs directly, without the involvement of CO_2 (i.e. the mechanism proposed by Schmidt et al.). Recently, we employed a pulse microreactor to study the OMS reaction over oxidized and reduced Rh catalysts.[13] The experimental results are consistent with the methane pyrolysis mechanism, in which $CH_{x,s}$ ($x = 0, 1, 2, 3$) fragments are the immediate precursors to syngas formation.

The catalytic OMS reaction is rather complex, and experimental conditions may influence the reaction steps strongly. From a survey of various studies,[1−13] one may agree that the contact time is an important factor which can affect the reaction schemes, as claimed by Schmidt et al.[6b] It is, therefore, expected that the shortening of the residence time can give rise to direct catalytic OMS. The methane dissociation mechanism may be supported by some surface science experiments. Ceyer et al.[14] have identified CH_3 on a Ni(111) surface with high-resolution electron energy loss spectroscopy, and Kaminsky et al.[15] have detected CH_3, CH_2, and CH intermediates on a Ni(111) methanation catalyst using static secondary ion mass spectrometry. On the basis of the methane pyrolysis mechanism, there are the following possible elementary steps (g = gas, s = surface):

* Corresponding author.
[†] Hong Kong Baptist University.
[‡] Xiamen University.

S1089-5639(97)03020-X CCC: $15.00
Published on Web 05/06/1998

$$O_{2,g} + \text{site} \rightarrow 2O_s \quad (2)$$

$$CH_{4,g} + \text{site} \rightarrow CH_{x,s} + (4 - x)H_s \rightarrow C_s + 4H_s \quad (3)$$

$$C_s + O_s \rightarrow CO_s \qquad \rightarrow CO_g \quad (4)$$

$$H_s + H_s \rightarrow H_{2,s} \qquad \rightarrow H_{2,g} \quad (5)$$

According to the results of pulse studies,[11,12] reduced metals were more favorable to CH_4 activation than oxides. Campbell et al.[16] reported that the reaction probability of methane on NiO films is significantly lower than that observed over a clean Ni(100) surface. Therefore, one can conclude that the reduced metal constitutes the main active site for syngas formation. Because atomic oxygen species are present on the catalysts (eq 2), the following reactions may be counted besides the steps (eq 3) proposed for the decomposition of CH_4:

$$CH_{4,s} + O_s \rightarrow CH_{3,s} + OH_s \quad (6)$$

$$CH_{x,s} + O_s \rightarrow CH_{x-1,s} + OH_s \quad (7)$$

$$O_s + H_s \rightarrow OH_s \quad (8)$$

Using the semiempirical bond-order conservation Morse potential (BOC-MP) approach, Hu and Ruckenstein[12a] calculated the activation energies for methane dissociation on Ni(111) with and without the involvement of surface oxygen. Oxygen located at on-top site was found to decrease the activation energy for the dehydrogenation of CH_x. It was therefore assumed that chemisorbed oxygen species have participated in the OMS reaction. The byproducts, CO_2 and H_2O, were detected during pulses of CH_4/O_2 mixture over the reduced catalysts. They may be generated according to reactions 9−11.

$$CO_g + O_s \rightarrow CO_{2,s} \rightarrow CO_{2,g} \quad (9)$$

$$CO_s + O_s \rightarrow CO_{2,s} \quad (10)$$

$$H_s + OH_s \rightarrow H_2O_s \rightarrow H_2O_g \quad (11)$$

Following the mechanisms shown above, we present here a detailed theoretical treatment of the OMS reaction on the transition and coinage metal (M) catalysts (M = Ni, Pd, Pt, Cu). On the basis of the assumption that reduced metals are the main active site, all effects of supporting materials on the reaction are neglected in the calculations. Experimentally, Ni was a significantly better OMS catalyst than Pd and Pt. Coinage metals are known to be far less active in OMS reaction than the transition metals. In our recent pulse studies,[11b,c] metallic copper did not activate methane; no CO and surface carbon were generated over Cu. Calculations on these systems would be of interest to evaluate the variation in catalytic abilities among these metals. Because it is difficult to locate transition states for the reactions on the metal surfaces, we focus here mainly on the thermodynamic aspects. We attempt to give theoretical evaluations of the surface reaction energies which should be important factors in determining the OMS processes. Experimental studies of methane dissociation cannot avoid the dynamic aspects. Knowledge of the barriers for methane dissociations can be useful in the understanding of the mechanism of the surface reactions. Our approach for estimating the activation energies is based on the actual calculations as well as on the analytic BOC-MP formalism. The BOC-MP model, developed by Shustorovich,[17] proved to be quite a useful theoretical model for treating surface dissociation or recombination.

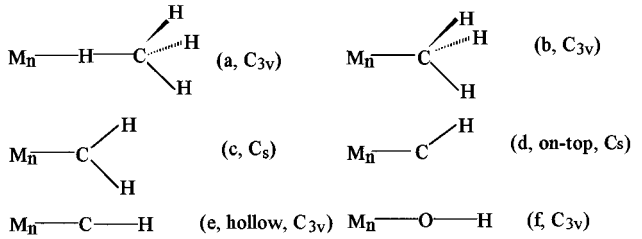

Figure 1. Models for the CH_x ($x = 4, ..., 1$) and OH species adsorbed on the metal cluster M_n.

There have been a number of theoretical studies of methane activation and methyl adsorption on Ni surfaces.[18−24] Relatively few theoretical studies have been devoted to the topics on other metal surfaces.[25−27] Theoretical investigations of methane activation over single atoms have also been reported.[28,29] The early studies were mainly concerned with the one-step dehydrogenation of methane to methyl. So far, no detailed theoretical treatments of the reactions involved in OMS have been reported in the literature.

2. Computational Details

2.1. Method of Computation. All calculations were carried out by the ADF (Amsterdam density functional) program system developed by Baerends et al.[30] The exchange-correlation potential used was based on the density-parametrized form of Vosko, Wilk, and Nusair (VWN).[31] The nonlocal corrections used were based on Becke's gradient functional for exchange[32] and Perdew's gradient functional for correlation.[33] Relativistic corrections of the valence electrons were calculated using the quasirelativistic method.[34] Concerning the basis sets, the triple-zeta STO basis sets were used for the metal ($n - 1$)d−ns, the C and O 2s−2p, and the H 1s valence shells. The orthogonalization wiggles of valence MOs were represented by optimized single-zeta STO sets. As usual, extra functions have been added to the valence bases: one p-type polarization function for transition and coinage metals, a 3d polarization function for C and O, and a 2p polarization function for H. The other shells of lower energy, i.e. [Ar] for Ni and Cu, [Kr] for Pd, and [Xe4f^{14}] for Pt, were considered as core shells and kept frozen according to the frozen-core technique.[30a]

2.2. Metal Surface Modeling. The structures of all the metals are equivalent. They crystallize in a ccp (cubic close packed) structure, where the atoms are distributed over the lattice points of the fcc (face-centered cubic) unit cell. At present, a M(111) plane was selected as the adsorption surface and was modeled by a two-layer-thick $M_{10}(n_1, 10 - n_1)$ cluster which contains n_1 metal atoms in the first layer and $10 - n_1$ metal atoms in the second. Here n_1 is 7 or 3, depending on the model (on-top or hollow site model) used. In practice, only a smaller two-layer-thick Ni_7 cluster was used for Ni(111) because we encountered the SCF convergence problem with the larger Ni_{10} cluster model. Therefore we have also presented here the calculated results on Pd_7 and Pt_7 so that the results on Ni(111) could be compared adequately with those on Pd(111) and Pt(111) within a same group. Furthermore, a larger M_{13} cluster was also tested for M = Pd and Cu in order to examine the influence of cluster size on the calculated results. With these clusters, the 3-fold symmetry axis is retained and there is computational advantage in most cases.

The models for the CH_x ($x = 4, ..., 1$) and OH species adsorbed on the metal surfaces are shown in Figure 1. The C atom in CH_3, CH_2, and CH has been placed to point toward the metal. The molecular parts above the metal surface are fully

optimized, where the symmetries for (a), (b), (e), and (f) are restricted to C_{3v}. The O−H bond is found to be perpendicular to the metal surface. For (c) and (d), C_s symmetry has been maintained for geometry optimization. All metal-metal distances are fixed to resemble those in the bulk of the metals. According to the pulse studies,[12,13] there are at least two possible pathways for methane dissociation, viz. direct dissociation and oxygen-assisted dissociation. Our calculations considered two types of adsorbed oxygen species (O_s) which are located at on-top and hollow sites.

3. Results and Discussion

3.1. Adsorption Properties of Species on Metal Surfaces. We begin with the chemisorptions of the CH_x ($x = 4, ..., 0$), H, and O species on the metal surfaces. Adsorption energies are major factors that determine the thermodynamics and dynamics of the CH_4 dissociation and syngas formation processes. Panas et al.[35] has suggested so-called "bond-prepared states" for calculating chemisorption energies of σ-bonded adsorbates. We do not choose to apply this method at present because we have not performed a systematic test of this rule within the ADF framework. The determination of adsorption sites has been a subject of theoretical studies.[20a,27,36] At present, only the on-top and the threefold hollow sites are considered. Table 1 presents a summary of the calculated adsorption energies together with the available experimental data on M(111)[17d] and BOC-MP results.[17d]

Let us first examine the cluster size effect. For Pd, three cluster sizes, i.e. Pd_7, Pd_{10}, and Pd_{13}, are investigated. As the cluster size is increased from Pd_7 to Pd_{10}, the calculated adsorption energies do not change significantly for most species. The difference (Δ) between the results on Pd_7 and Pd_{10} is relatively large for H $\rightarrow$ O^{top}, Δ being 0.9 eV. Another point should be mentioned. For CH_3 on Pd_7, the calculated adsorption energy at the on-top site is close to that at the hollow site, but there is a strong preference for the on-top site on Pd_{10}. The same strong preference for the on-top site is also found on Pd_{13}, Ni (Ni_7), and Pt (Pt_7, Pt_{10}). The adsorption energies calculated on Pd_{13} are close to those on Pd_{10}. for M = Pt, the results of CH_x and H on Pt_7 are also quite close to those on Pt_{10}. The results of O and OH on Pt_7 are similar to those on Pt_{10}, but correspond to different preferred sites. The preferred sites of O on Ni_7, Pd_{10} (Pd_{13}), and Pt_{10} are the same and they are in agreement with the known fact that O favors hollow site on metal.[17d] For the adsorption of OH, the calculations with the M_7 clusters all yield a preferred on-top site and the calculations with M_{10} give the opposite situation. For OH on Pd_{10}, however, there is a slight preference for the hollow site. The BOC-MP model predicts that the hollow site is preferred for OH,[17d] in agreement with the results calculated on the M_{10} clusters. The OH species is the only exception for Ni_7 which gives different preferred site than Pd_{10} or Pt_{10}. For M = Cu, the M_{10} and M_{13} clusters give also similar results.

From these calculated results, we may conclude that the M_{10} cluster is suitably large and Ni_7 is adequate to give reliable results. In the next subsections, we discuss the adsorption properties of the species individually. Unless otherwise stated, we will rely on the results calculated with the Ni_7 and M_{10} clusters. When a comparison is made among the transition metals, the cluster size effect has already been taken into account. To facilitate comparison of the calculated adsorption energies (E) among the various CH_x species and the different metals (M), plots of E versus x and M are shown in Figure 2. The plots of E for O and H are shown in Figure 3. Table 2 gives the calculated heights of the species above the metal surfaces. We have not listed out the other calculated geometry parameters. It was found that the C−H and O−H bond lengths only change very slightly from the free species to the adsorbed ones and the umbrella angles in adsorbed CH_4 and CH_3 are equal or nearly equal to the tetrahedral one. Table 3 gives the Mulliken charge distributions on the whole adsorbed species.

3.1.1. Adsorbed CH_4. The adsorption energies, E, of CH_4 are found to be very small on all the metal surfaces investigated. The calculated energies are even negative for some of the hollow sites. This is to be expected because CH_4 is a saturated molecule and is very stable. The on-top site seems to be more favorable for the adsorption of CH_4. The Ni−H and Cu−H distances are calculated to be about 2.3 Å. These distances are smaller than the sum of the van de Waals radii[37] (R^{vdW}_{Ni+H} = 2.80 Å, R^{vdW}_{Cu+H} = 2.60 Å) but much larger than the sum of the Pauling's covalent radii (R^{cov}_{Ni+H} = 1.47 Å, R^{cov}_{Cu+H} = 1.49 Å). It is interesting to realize that the metal−H distances decrease in the order Ni−H > Pd−H > Pt−H. The C−H bonds to the surface stretch by 0.01, 0.02, and 0.03 Å for M = Ni, Pd, and Pt, respectively, corresponding to the decrease in the M−H distances. The relativistic effects increase the Pt−H bond strength "significantly" and cause a remarkable Pt−H bond contraction. There is also a small charge transfer from Pt_n to the adsorbate due to the close approach. On the other metal clusters, the charge transfer occurs from the adsorbed species to M_n.

3.1.2. Adsorbed CH_3. CH_3 is a relatively strongly bound radical. It prefers the on-top sites when adsorbed on the transition metals, the difference in the adsorption energies between on-top and hollow sites being about 0.4−0.6 eV. The CI calculations by Schüle et al.[20a] as well as by Yang and Whitten[21a] yielded a slightly preferred hollow site for CH_3 on Ni(111). Our calculated E of 2.2 eV for CH_3 on Ni(111) is quite close to the contracted CI value of 2.0−2.2 eV[20a] which was calculated using the varying cluster models and the so-called "bond-prepared" states.[35] These results also agree well with the BOC-MP value. The M−C bonds are relativistically stabilized. The relativistic contributions are 0.07, 0.13, and 0.44 eV for M = Ni, Pd, and Pt, respectively, changing the nonrelativistic order of E^{nrel}(Ni) > E^{nrel}(Pd) > E^{nrel}(Pt) to E^{rel}(Ni) > E^{rel}(Pt) > E^{rel}(Pd). The calculated M−C distances for the on-top site are close to the sum of Pauling's covalent radii. Electron transfer from the metal to the CH_3 group is significant and the total negative charge Q on the group increases from M = Ni to M = Pt.

For CH_3 on the coinage metal Cu, the hollow site is more favorable, the on-top site being about 0.5 eV less stable than the hollow site. The calculated adsorption energy is smaller than those on the transition metals. Nearly no change in the population takes place from free CH_3 to the adsorbed one.

3.1.3. Adsorbed CH_2, CH, and C. For the adsorptions of CH_2, CH, and C, the hollow site is clearly preferred. There are major differences in the adsorption energies of these species at the on-top and hollow sites. On the other hand, the energy difference $\Delta^{top-hol}$ is much more pronounced for CH or C than for CH_2.

The calculated adsorption energy of 7.65 eV for C on Ni is in good agreement with the experimental value of 7.42 eV. No corresponding experimental measurements have been reported for C on the heavier transition metals. Two assumed experimental values of 6.94 and 6.50 eV were given by Shustorovish for Pd and Pt, respectively. The corresponding calculated results are 6.65 and 7.40 eV, showing reasonable agreements with the

TABLE 1: Calculated Adsorption Energies *E* (eV) for the Various Species Adsorbed on the $M_n(n_1,n_2)$ Cluster Models of M(111) (M = Ni, Pd, Pt, Cu)[a]

(a) On Ni_7

	Ni(1,6) (top)	Ni(6,1) (hol)	expt	CCI[b] (hol)	BOC-MP (hol)
CH_4	*0.09* (0.07)	0.01			
CH_3	*2.21* (2.14)	1.76		1.95−2.17	2.08
CH_2	3.34	*4.52* (4.50)			3.60
CH	5.03	*7.14* (7.13)			5.03
C	4.77	*7.65* (7.58)	7.42		
H	2.30	*2.97* (2.97)	2.73	2.43−2.52	
O	4.79	*5.59*	4.99		
H→O[c]	*3.66*	1.76			
OH	*3.49*	2.39			2.65

(b) On Pd_7, Pd_{10}, and Pd_{13}

	Pd(1,6) (top)	Pd(6,1) (hol)	Pd(7,3) (top)	Pd(3,7) (hol)	Pd(7,6) (top)	Pd(7,6) (hol)	expt	BOC-MP (hol)
CH_4	0.08	−0.12	*0.04* (0.03)	0.02	0.02	0.01		
CH_3	1.31	1.33	*1.54* (1.41)	1.12	1.66	1.07		1.82
CH_2	2.33	3.54	2.14	*3.45* (2.99)	2.61	3.28		3.25
CH	3.38	6.26	3.60	*5.74* (4.79)	3.26	6.19		4.60
C	3.75	6.37	4.43	*6.67* (6.05)	4.19	6.82	[6.94][d]	
H	1.73	2.94	2.35	*2.61* (2.48)	2.46	2.70	2.69	
O	2.82	3.99	3.15	*4.09*	2.71	4.23	3.77	
H→O	4.19	2.39	*3.32*	2.51	3.45	2.88		
OH	2.06	1.43	1.52	*1.65*	1.15	2.16		1.73

(c) On Pt_7 and Pt_{10}

	Pt(1,6) (top)	Pt(6,1) (hol)	Pt(7,3) (top)	Pt(3,7) (hol)	expt	BOC-MP (hol)
CH_4	0.18	−0.11	*0.14* (0.05)	−0.05		
CH_3	1.75	0.65	*1.77* (1.33)	1.23		1.65
CH_2	3.48	3.33	3.03	*3.66* (2.74)		2.95
CH	4.56	6.27	3.80	*6.71* (5.34)		4.21
C	5.33	6.75	4.61	*7.40* (6.38)	[6.50][e]	
H	2.23	2.84	2.44	*2.59* (1.99)	2.65	
O	4.08	3.14	2.71	*4.24*	3.69	
H→O	3.44	2.84	*3.34*	2.91		
OH	2.56	1.02	1.09	*2.20*		1.69

(d) On Cu_{10} and Cu_{13}

	Cu(7,3) (top)	Cu(3,7) (hol)	Cu(7,6) (top)	Cu(6,7) (hol)	expt
CH_4	*−0.09*	−0.13	−0.10	−0.11	
CH_3	0.65	*1.15*	0.81	1.28	
CH_2	1.23	*3.01*	1.57	2.75	
CH	1.70	*4.50*	2.17	4.51	
C	1.45	*3.73*	2.17	3.89	[5.20][f]
H	1.32	*2.12*	1.58	2.28	2.43
O	2.28	*5.07*	2.58	4.67	4.47
H→O	*4.49*	2.67	4.21	3.12	
OH	1.82	*2.79*	1.84	2.94	

[a] The adsorption energies of the species adsorbed at the preferred site are indicated in italic. The values in brackets are the nonrelativistic results. (Experimental data on M(111) are those cited in ref 17d). [b] Contracted CI calculation by Schüle et al.[20a] using the varying cluster models and the so-called "bond-prepared" states. [c] Represents adsorption of H on surface O and hereafter. [d] Assumed experimental value.[17d] [e] Assumed experimental value.[17d] [f] Assumed experimental value.[17d]

assumed values. However, the orders of the energies are different. The calculation shows the order of E_C's: Pd < Pt. For C on Cu, the calculated E_C is considerably smaller than the assumed experimental value.

No experimental data are available for the adsorbed CH_2 and CH species. The calculated *E* values for CH are significantly larger than the BOC-MP estimates. The *E* values vary in the order of Ni > Pt > Pd, similar to the C and CH_3 cases. Within the three species, the adsorption energies follow the ordering of CH_2 < CH < C for the transition metals. The increase in the adsorption energies corresponds to the decrease in the M(hollow)−C distances along the series. In the case of Cu, however, there is an abnormal order of *E*'s: CH_2 < C < CH. It is interesting that the Cu(hollow)−CH distance is also smaller than the Cu(hollow)−C distance. On all the metals, the change in E from CH_2 to CH is very large, up to a ΔE value of 2−3 eV. The relativistic stabilization in the M(hollow)−CH_x bond increases in the order of CH > C > CH_2. There is a very large relativistic increase in the adsorption energy of CH on Pt. Pd(hollow)−CH is also seen to be significantly stabilized. Because of the small atomic number of Ni, the relativistic adsorption energies are close to those obtained in the nonrelativistic calculations.

The Pd(hollow)−CH_x distances are quite similar to the Pt(hollow)−CH_x ones. Nonrelativistically, Pt(hollow)−CH_x is clearly larger than Pd(hollow)−CH_x. The relativistic 'bond'

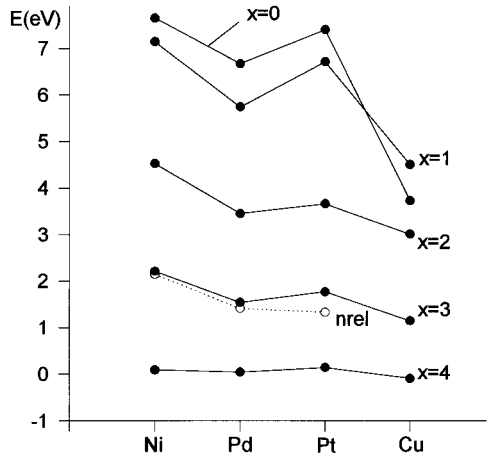

Figure 2. Schematic illustration of calculated adsorption energies for the CH_x species on the metal M(111) surfaces.

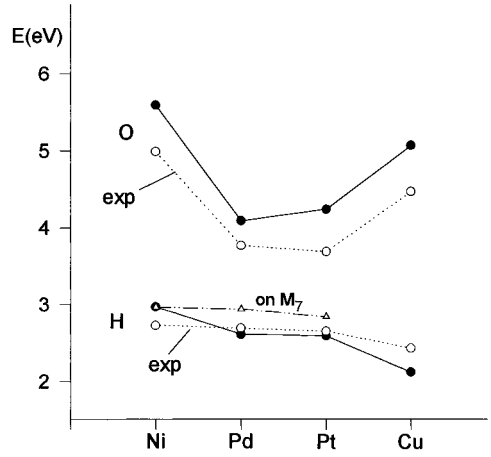

Figure 3. Schematic illustration of calculated adsorption energies for the H and O species on the metal M(111) surfaces. The open circles represent experimental data.

TABLE 2: Calculated Heights[a] (Å) above the Metal Surface (Values in Brackets are the Nonrelativistic Results)

		Ni_7	Pd_{10}	Pt_{10}	Cu_{10}
CH_4	on-top	2.29 (2.29)	2.10 (2.16)	2.05 (2.20)	2.29
	hollow	2.29	2.15	2.10	2.29
CH_3	on-top	1.91 (1.93)	2.04 (2.08)	2.08 (2.15)	2.07
	$\sum R_{cov}$[b]	1.92	2.05	2.07	1.94
	hollow	1.53	1.73	1.73	1.65
CH_2	on-top	1.77	1.88	1.90	1.93
	hollow	1.23 (1.25)	1.35 (1.39)	1.43 (1.55)	1.40
CH	on-top	1.65	1.81	1.79	1.88
	hollow	1.06 (1.07)	1.09 (1.14)	1.12 (1.25)	1.19
C	on-top	1.59	1.74	1.77	1.82
	hollow	1.00 (1.01)	1.03 (1.07)	1.06 (1.20)	1.24
H	on-top	1.50	1.53	1.59	1.54
	hollow	0.81 (0.83)	0.78 (0.82)	0.79 (0.93)	0.94
O	on-top	1.61	1.82	1.85	1.80
	$\sum R_{cov}$[b]	1.88	2.01	2.03	1.90
	hollow	1.05	1.20	1.21	1.22
HO	on-top	1.73	2.04	2.08	1.94
	hollow	1.40	1.62	1.65	1.46

[a] The heights calculated on Pd_7 and Pt_7 are similar to those on Pd_{10} and Pt_{10}, and so they are not listed here. [b] Pauling's covalent radii.

contractions of M(hollow)−CH_x are about 0.01, 0.05, and 0.13 Å for M = Ni, Pd, and Pt, respectively. The CH_x group is calculated to be rather negative. The negative charge $\sum Q$ on the CH_x group increases in the order of Ni < Pd < Pt. The atomic electronegativity rule is not relevant to the calculated charges.

TABLE 3: Mulliken Charge Distributions (in e) on the Whole Adsorbed Species

		Ni_7	Pd_7	Pt_7	Pd_{10}	Pt_{10}	Cu_{10}
CH_4	on-top	0.05	0.05	−0.17	0.15	−0.08	0.18
	hollow	0.05	0.17	−0.09	0.30	−0.02	0.14
CH_3	on-top	−0.14	−0.42	−0.60	−0.32	−0.40	0.00
	hollow	0.07	−0.64	−0.33	−0.64	−0.78	−0.02
CH_2	on-top	−0.13	−0.50	−0.79	−0.41	−0.49	−0.04
	hollow	−0.17	−0.98	−1.36	−1.02	−1.32	−0.46
CH	on-top	−0.30	−0.48	−0.78	−0.46	−1.04	−0.11
	hollow	−0.38	−1.24	−1.91	−1.27	−1.72	−0.79
C	on-top	−0.24	−0.35	−0.55	−0.33	−0.55	−0.10
	hollow	−0.31	−0.92	−1.26	−0.89	−1.30	−0.51
H	on-top	−0.18	−0.36	−0.07	−0.40	−0.24	−0.14
	hollow	−0.02	−0.69	−0.77	−0.82	−0.89	−0.07
O	on-top	−0.64	−0.57	−0.61	−0.54	−0.54	−0.65
	hollow	−0.64	−0.88	−0.84	−0.86	−0.98	−0.82
HO	on-top	−0.36	−0.48	−0.58	−0.44	−0.44	−0.45
	hollow	−0.30	−0.39	−0.28	−0.59	−0.48	−0.43

3.1.4. Adsorbed H and O. H clearly prefers the hollow site, in agreement with other calculations.[20a,21,24] The calculated adsorption energies are quite close to the experimental estimates, the error being less than 0.3 eV. The relativistic contributions to the adsorption energies are 0, 0.13, and 0.60 eV for M = Ni, Pd, and Pt, respectively. The experiments show that there is no obvious trend in the E_H's among the transition metals. The calculations show that the adsorption energy of H on Ni are about 0.4 eV larger than on Pd and Pt. In order to compare with the experimental trend, the cluster size effect has to be taken into account. The calculations on Pd_7 and Pt_7 show that the M_7 cluster may give an adsorption energy which is about 0.3 eV larger than M_{10}. A notable fact is that the values of the adsorption energy of H are much smaller than the energy required for the breakage of a tetrahedral CH bond (4.85 eV^{calc}, 4.51 eV^{exp}). Hence, the generation of gas-phase CH_3 via H abstraction from CH_4 is difficult on the metal surfaces. An experimental evidence is the fact that spontaneous desorption of unsaturated species was not observed over Pt catalysts at temperatures of the experiments.[38] This is in contrast to the oxidative coupling of methane (OCM) reaction on metal oxides, where gas-phase methyl radicals could be produced easily.[39−41] The formation of methyl radicals over MgO in the gas-phase has been confirmed using argon matrix trapping.[42] However, one cannot rule out the possibility for the combination of adsorbed CH_3 species: $CH_{3,s} + CH_{3,s} \rightarrow C_2H_{6,g}$, which competes with the dissociation processes and is also dominated by the reaction energy. Experiments[38] showed that the coupling involving CH_x species deriving from CH_4 adsorption could indeed take place. Section 3.3 discusses the couplings of the surface $CH_{x,s}$ species.

O prefers the hollow site of the metal surfaces. For O on Pt, the cluster size effect has been found to be significant. The calculations on the smaller Pt_7 cluster show that O is more strongly bound at the on-top site than at the hollow site, disagreeing with the general trend. The calculated adsorption energies exceed the experimental data by 0.3−0.6 eV. The $M-O^{top}$ distances are all shown to be significantly smaller than the sums of Pauling's covalent radii, indicating a strong covalent bonding between the metal and O. The net charge on O at the hollow site is higher than that at the on-top site.

Adsorption of H on surface O, results in the formation of OH_s. The surface−O distances are significantly expanded after H adsorption, the expansion of $M-O^{hol}$ being much more pronounced than the expansion of $M-O^{top}$. The calculated adsorption energies of H depend strongly on the position at which the O is located. The adsorption energies $E(H \rightarrow O)$ of

H at O^{top} are considerably larger than those at O^{hol}. So the oxygen adsorbed at a metal on-top site has a stronger tendency to form a single bond than that at a hollow site. The $E(H\rightarrow O^{top})$ values are also larger than the adsorption energies of H on bare metal surfaces, i.e. HO_s^{top} is more stable than H_s. HO_s^{hol} may be more or less stable than H_s, depending on the metal (see Table 5).

3.1.5. Summary. Free CH_4 is only weakly bound to the metal surfaces and the on-top site is more preferred than the hollow site for CH_4 adsorption. The CH_3 radical adsorbs rather strongly to the metals. The ground chemisorption state for CH_3 can correspond to both on-top and hollow sites, depending on the metal. This disagrees with the BOC-MP estimates[36] and the extended Hückel band results.[27] According to the predictions of the BOC-MP model, the hollow site is typically preferred for CH_3, while the extended Hückel band calculations indicated the reversed order for CH_3, i.e. on-top > hollow. The ordering in the adsorption energies of CH_3 on the transition metals is Ni > Pt > Pd. The reverse order of E's from Pd to Pt is caused by the relativistic effects. The calculated adsorption energy of CH_3 on Cu(111) is 1.2−1.3 eV, much smaller than that on Ni and also smaller than those on Pd and Pt.

For CH_2, CH, and C, the hollow site is always preferred. The difference in the adsorption energies between the on-top and hollow sites is large. Therefore, unsaturated C in these species has a strong tendency to recover its missing bonds, in agreement with the extended Hückel band prediction.[27] The adsorption energy of CH_x on a given transition metal increases from $x = 3$ to $x = 0$. The increase is large from CH_2 to CH but is much less from CH to C. On Cu, C has the adsorption energy which is smaller than that of CH. The variation of the adsorption energy with metal for CH_x is similar to that for CH_3.

H typically prefers the hollow site. The calculated adsorption energies are about 2.6−3.0 eV (expt, ∼2.7 eV) and 2.1−2.3 eV (expt, 2.4 eV) for the transition metals and Cu, respectively. There is no obvious trend in E for monovalent H within the series Ni−Pd−Pt. So the adsorption properties of CH_3 and H on the transition metals are in fact quite different. Because the C−H bond strength in CH_4 is much stronger than the adsorption energies of H, no methyl radicals would be formed in the gas phase by the dissociation of methane on the metal surfaces. This could explain why the dissociation of methane on the metal catalysts leads mainly to syngas rather than higher carbon products.

The adsorption energies for O are rather large. So O can be firmly trapped on the metal surfaces. H can bind on O_s^{top} more strongly than on the bare metals. So the H species produced in methane dissociation may react with O_s to form OH_s.

3.2. Methane Dissociation on Metal Surfaces. The calculated adsorption energies given in Table 1 together with the calculated C−H bond strengths in the gas-phase $CH_{x,g}$ have been used to determine the dissociation energy $D_{AB,s}$ for $CH_{x,s}$ dissociation on the metal surfaces. The scheme is shown as follows:

$$\begin{array}{ccc} CH_{x,s} & \xrightarrow{D_{AB,s}} & CH_{x-1,s} + H_s \\ \uparrow -E_{AB} & & \uparrow -E_A \quad \uparrow -E_B \\ CH_{x,g} & \xrightarrow[D_{AB,g}]{} & CH_{x-1,g} + H_g \end{array} \qquad (12)$$

$$D_{AB,s} = D_{AB,g} + E_{AB} - E_A - E_B \qquad (13)$$

where AB, A, and B correspond to CH_x, CH_{x-1}, and H, respectively. We use symbols AB, A, and B for the subscripts in order to be consistent with those in the following formulae.

The calculated results for $D_{CH_{x,s}}$ on the metals studied are collected in Table 4, together with the results for $O_{2,g} \rightarrow O_s + O_s$. Equation 13 indicates that $D_{CH_{x,s}}$ can be expressed as a combination of the four energy terms. E_H is seen to be significantly smaller than $D_{CH_{x,g}}$. Therefore, the relative adsorption energy $E_{CH_x} - E_{CH_{x-1}}$ plays an important role in determining the ease of dissociation of the surface $CH_{x,s}$ species.

In order to estimate the barrier heights, the bond-order conservation Morse potential (BOC-MP) approach developed by Shustorovich[17] is employed here to evaluate the activation energies. The analytic BOC-MP formula relates the activation energy E^* to the adsorption energies of an adsorbate and its dissociative fragments on the surface. For a dissociation on a metal surface,

$$AB_s \rightarrow A_s + B_s \qquad (14)$$

the formula is given by

$$E^*_{AB,s} = {}^1/_2\left(D_{AB,g} + \frac{E_A E_B}{E_A + E_B} + E_{AB} - E_A - E_B\right)$$

$$= {}^1/_2\left(\frac{E_A E_B}{E_A + E_B} + D_{AB,s}\right) \qquad (15)$$

where $D_{AB,g}$ is the dissociation energy of A−B in the gas phase; E_{AB} is the energy of chemisorption for molecular adsorbate AB; and E_A and E_B are the energies of chemisorption of the atoms or atomic groups A and B, respectively.

Within the BOC-MP framework, the values of $D_{AB,g}$, E_A, and E_B are not calculated but taken from experiments, and the evaluation of E_{AB} is also based on $D_{AB,g}$ and E_A (or E_B). We now solely use our ADF results for these energy terms to estimate the activation energies. From eq 15, we see that the activation energy for surface dissociation can be directly and simply related to the dissociation energy of the surface reactant. Hence, a larger negative dissociation energy will give rise to a lower barrier height and vice versa. The plots of $D_{CH_{x,s}}$ and E^* on the different metals are shown in Figures 4 and 5, respectively.

3.2.1. Dissociation of O_2. At first, we examined the dissociation of O_2 on the metal surfaces. In the molecular state, the adsorbed O_2 species were assumed to lie parallel to the surface.[43] We have not calculated the adsorption energy of molecular O_2. The dissociations of $O_{2,g}$ to $2O_s$ on the metals are seen to be rather exothermic, especially on Ni. Therefore, atomic oxygens can be generated easily on the metals by dissociative adsorption of gas-phase oxygen. This conclusion is in concord with the pulse experimental results over supported metal catalysts.[12]

3.2.2. Dissociations of CH_x. Many experimental studies have been devoted to methane activation on clean Ni surfaces (see references cited in ref 16). An apparent activation energy of 12.0 kcal/mol (0.52 eV) for the dissociative chemisorption of CH_4 on Ni(111) was obtained by Ceyer et al.[14b,44] using molecular beam techniques coupled with high-resolution electron energy-loss spectroscopy. Beebe et al.[45] obtained a slightly higher barrier (12.6 kcal/mol = 0.55 eV). The calculated value of 0.52 eV is found to be in good agreement with the experimental data. Other calculations on clusters give significantly higher barrier heights (0.74,[21b] 1.25,[22b] 0.97,[23] and 1.04 eV[24]). The barrier for Ni atom insertion was determined to be 0.42 eV.[29] The first dehydrogenation step $CH_{4,s} \rightarrow CH_{3,s} + H_s$

TABLE 4: Calculated Dissociation Energies $D_{AB,s}$ (Eq 12) and Activation Energies E^* (Eq 15) for Direct Dissociation of the CH_x Species (x = 4, 3, 2, 1) on the M(111) Surface (M = Ni, Pd, Pt, Cu) (Values in Brackets Are the Nonrelativistic Results; All Energies Are in eV; g = Gas, s = Surface)

	$D_{AB,g}$	E_{AB}	$-E_A$	$-E_B$	$D_{AB,s}$	μ_E[a]	$E^*_{AB,s}$[b]
(a) M = Ni (on Ni_7)							
$O_{2,g} \rightarrow O_s + O_s$	6.57	–	−5.59	−5.59	−4.61		
$CH_{4,s} \rightarrow CH_{3,s} + H_s$	4.85	0.09	−2.21	−2.97	−0.24 (−0.09)	1.27	0.52
$CH_{3,s} \rightarrow CH_{2,s} + H_s$	5.13	2.21	−4.52	"	−0.15 (−0.30)	1.79	0.82
$CH_{2,s} \rightarrow CH_s + H_s$	4.93	4.52	−7.14	"	−0.66 (−0.67)	2.10	0.72
$CH_s \rightarrow C_s + H_s$	3.72	7.14	−7.65	"	0.24 (0.30)	2.14	1.19
$CH_{4,s} \rightarrow C_s + 4H_s$					−0.81 (−0.76)		
(b) M = Pd (on Pd_{10})							
$O_{2,g} \rightarrow O_s + O_s$	6.57	–	−4.09	−4.09	−1.61		
$CH_{4,s} \rightarrow CH_{3,s} + H_s$	4.85	0.04	−1.54	−2.64	0.71 (0.99)	0.97	0.84
							0.79[c]
							0.77[d]
$CH_{3,s} \rightarrow CH_{2,s} + H_s$	5.13	1.54	−3.45	"	0.58 (1.07)	1.50	1.04
							0.80[c]
							1.15[d]
$CH_{2,s} \rightarrow CH_s + H_s$	4.93	3.45	−5.74	"	0.00 (0.65)	1.81	0.91
							0.64[c]
							0.60[d]
$CH_s \rightarrow C_s + H_s$	3.72	5.74	−6.67	"	0.15 (−0.02)	1.89	1.02
							1.34[c]
							1.16[d]
$CH_{4,s} \rightarrow C_s + 4H_s$					1.44 (2.69)		
					0.58[c]		
					1.06[d]		
(c) M = Pt (on Pt_{10})							
$O_{2,g} \rightarrow O_s + O_s$	6.57	–	−4.24	−4.24	−1.91		
$CH_{4,s} \rightarrow CH_{3,s} + H_s$	4.85	0.14	−1.77	−2.59	0.63 (1.62)	1.05	0.84
							0.76[e]
$CH_{3,s} \rightarrow CH_{2,s} + H_s$	5.13	1.77	−3.66	"	0.65 (1.68)	1.52	1.09
							1.06[e]
$CH_{2,s} \rightarrow CH_s + H_s$	4.93	3.66	−6.71	"	−0.71 (0.39)	1.87	0.58
							0.63[e]
$CH_s \rightarrow C_s + H_s$	3.72	6.71	−7.40	"	0.44 (0.69)	1.92	1.18
							1.20[e]
$CH_{4,s} \rightarrow C_s + 4H_s$					1.01 (4.38)		
					0.70[e]		
(d) M = Cu (on Cu_{10})							
$O_{2,g} \rightarrow O_s + O_s$	6.57	–	−5.07	−5.07	−3.57		
$CH_{4,s} \rightarrow CH_{3,s} + H_s$	4.85	0.02	−1.15	−2.12	1.60	0.75	1.12
							1.01[f]
$CH_{3,s} \rightarrow CH_{2,s} + H_s$	5.13	1.15	−3.01	"	1.15	1.24	1.20
							1.31[f]
$CH_{2,s} \rightarrow CH_s + H_s$	4.93	3.01	−4.50	"	1.32	1.44	1.38
							1.20[f]
$CH_s \rightarrow C_s + H_s$	3.72	4.50	−3.73	"	2.37	1.35	1.86
							1.75[f]
$CH_{4,s} \rightarrow C_s + 4H_s$					6.44		
					5.52[f]		

[a] $\mu_E = E_A E_B/(E_A + E_B)$ and hereafter. [b] $E^*_{AB} = {}^1/_2(\mu_E + D_{AB,s})$. [c] Values calculated on the Pd_7 cluster. [d] Values calculated on the Pd_3 cluster. [e] Values calculated on the Pt_7 cluster. [f] Values calculated on the Cu_{13} cluster.

on Ni is mildly exothermic (by 0.24 eV), thereby proceeding easily. Similar finding was reported from CI cluster calculations by Yang and Whitten,[21b] who obtained an exothermicity for this reaction of 0.13 eV. Experimentally the reaction is found to be slightly exothermic.[14b] The subsequent dissociations of CH_3 and CH_2 on Ni are exothermic by 0.2 and 0.7 eV, respectively. The related activation energies are estimated to be 0.8 and 0.7 eV. The last step dissociation (i.e. $CH_s \rightarrow C_s + H_s$) is endothermic by 0.24 eV and the activation energy is relatively high (1.2 eV). The activation energy of the CH_4 dehydrogenation on Pd is notably higher than on Ni (by about 0.3 eV). Pt(111) and Pd(111) show close activation energies for the first dehydrogenation step. On Pt, the third dehydrogenation step is mildly exothermic and has a relatively low activation energy, but the other reaction steps are mildly endothermic. On Pd, the first and second steps are mildly endothermic, while the other two steps are nearly thermoneutral.

Concerning the activation energies E^*, there are also no consistent trends within the transition metals. From these results, it seems hard to predict the trend in the catalytic activities within the transition metals. Therefore we lumped the elementary steps into one $CH_{4,s} \rightarrow C_s + 4H_s$ step and calculated the total dissociation energy $D^{tot}_{e,s}$. From the $D^{tot}_{e,s}$ values obtained (see Table 4 and Figure 4), the total dissociation is found to be quite exothermic on Ni (by 0.8 eV), while it is rather endothermic on Pd (by 1.4 eV) and Pt (by 1.0 eV). Although the M_7 cluster gives lower dissociation energies (0.6 eV for Pd_7, 0.7 eV for Pt_7) than M_{10}, the overall trend is not altered. The trend in the $D^{tot}_{e,s}$ values is in concord with the experimental fact[6] that CH_4 conversion on Ni was significantly higher than Pd and Pt, and both Pd and Pt showed similar CH_4 conversion. Therefore, a correlation does exist between the total dissociation energy and catalytic activity. The relativistic effects are found

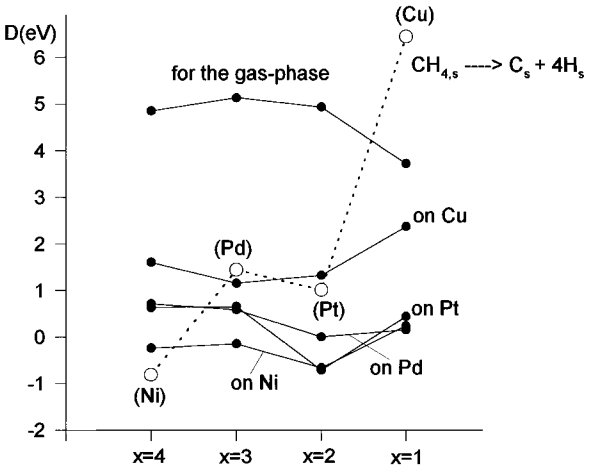

Figure 4. Schematic illustration of calculated dissociation energies for the CH_x dissociation on the metal M(111) surfaces. The calculated dissociation energies for the gas-phase $CH_{x,g}$ (top curve) are given for comparison. The open circles represent the total dissociation energies for the complete dissociation of methane ($CH_{4,s} \rightarrow C_s + 4H_s$).

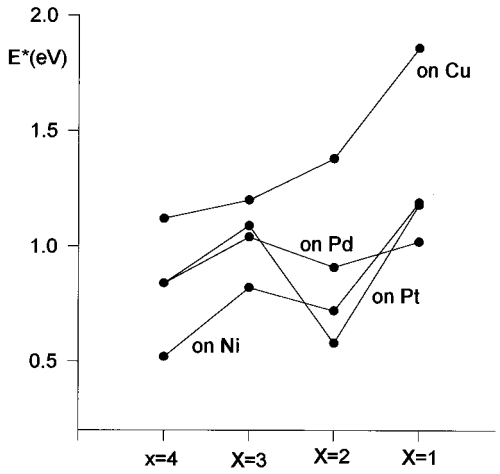

Figure 5. Schematic illustration of calculated activation energies for the CH_x dissociation on the metal M(111) surfaces.

to support the methane dissociations and increase strongly from M = Ni to Pt.

Let us take a look at the dissociations of $CH_{x,s}$ on Cu. All the discrete dissociation steps, especially the last $CH_s \rightarrow C_s + H_s$ step, are rather endothermic and the total dissociation is found to be very endothermic. There are two causes for the high endothermicity. On one hand, the adsorption energy of H on Cu is relatively small as compared with those on the transition metals. On the other hand, the adsorption energy of CH_x on Cu increases only weakly from $x = 3$ to $x = 1$ and even decreases from $x = 1$ to $x = 0$. The activation energies for the dissociation of CH_x on Cu are also significantly higher than that on the transition metals. Therefore no surface C species are expected to be generated over Cu, in agreement with the experimental fact that surface C species are rarely detected over Cu.[11b,c] In other words, the complete dissociation of CH_4 on Cu catalysts is very difficult. This explains why Cu catalysts are inactive in the OMS reaction.

3.2.3. Oxygen-Assisted Dissociations. We now turn to examine the oxygen-assisted dissociations. The results are given in Table 5, where Δ represents the difference between the dissociation energies with and without the involvement of chemisorbed oxygens. Compared to the direct dissociations of methane on bare metal surfaces, the methane dissociations involving O_s located at on-top site have significantly lower dissociation energies. This means that O_s^{top} promotes the dehydrogenation of CH_x. On Cu, the dissociations of $CH_{x,s}$, with $x = 4$, 3, 2, in the presence of O^{top} become rather exothermic, and the last dissociation step, $CH_s \rightarrow C_s + H_s$, is now nearly thermoneutral. The Δ^{top} values are similar for the transition metals (~ -0.7 eV); it is very negative for Cu (-2.4 eV). However, the O species at the metal hollow site, O_s^{hol}, shows different behavior towards methane dissociation. The Δ^{hol} value may be positive or negative, depending on the metal. On Pt and Cu, O_s^{hol} also promotes methane dissociation, but less pronouncedly than O_s^{top}. On Ni and Pd, O_s^{hol} is not beneficial to methane dissociation. There were BOC-MP calculations of activation energies for the methane dehydrogenation on Ni with and without the involvement of surface oxygen.[12a] The same conclusion was also drawn there. The Δ^{hol} value decreases along the series: Ni(1.21 eV) > Pd(0.13 eV) > Pt(-0.32 eV) > Cu(-0.55 eV). According to the calculated results, significant methane dissociation on Cu would be possible if the Cu surface is occupied by a large amount of oxygen. This is in parallel with the experimental fact that methane reacts with supported CuO to produce CO_2 and H_2O.[11b,c]

3.3. Syngas and Byproducts Formation. *3.3.1. H_2, CO, CO_2, and H_2O Formation.* According to the methane pyrolysis mechanism, adsorbed H atoms combine to form H_2 and adsorbed C_s reacts with O_s to produce CO, which desorbs before being further oxidized. On the other hand, gas-phase CO may be further oxidized by surface O_s to produce CO_2, whereas OH_s may combine with H_s to form H_2O. Shustorovich[17d] gave a formula similar to eq 15 for the reverse reaction of recombination of chemisorbed A and B:

$$E^*_{A+B,s} = {}^1/_2\left(\frac{E_A E_B}{E_A + E_B} + E_A + E_B - D_{AB,g} - E_{AB}\right)$$

$$= {}^1/_2\left(\frac{E_A E_B}{E_A + E_B} + C_{A+B,s}\right) \qquad (16)$$

where $C_{A+B,s}$ is the combination energy for $A_s + B_s \rightarrow AB_s$. The formula is also applied here to calculate the activation energies for $H_s + H_s \rightarrow H_{2,s}$ and $C_s + O_s \rightarrow CO_s$. The calculated combination and desorption energies are summarized in Table 6, together with the calculated activation energies. Here we have not presented the results based on the Pd_7 and Pt_7 clusters. It is found that the drawn conclusions do not change with use of these clusters.

On Ni, additional energy of about 1.1 eV is required for the combination reaction of $H_s + H_s$. Kratzer et al.[24] calculated that H_2 dissociation on Ni(111) is exothermic by 1.00 eV. An experimental value for the H_2 dissociation energy on Ni(111) is 0.99 eV.[46] These data are in good agreement with our calculated value on Ni. There is also relatively high activation energy (1.3 eV) for the combination. Therefore, the formation of H_2 on the transition metals may only take place at relatively high temperature. The combination of $H_s + H_s$ on Pd and Pt is less endothermic than on Ni. The combination reaction on Cu is exothermic, owing to the relatively small adsorption energy of H on Cu. The calculated desorption energies of H_2 are all nearly zero. This means that once H_2 is formed on the metals, the subsequent desorptions are easy.

The calculated combination energies of $C_s + O_s$ vary greatly with the metals. C_s and O_s can combine very easily on Pd and Pt. The combination of $C_s + O_s$ on Ni is mildly exothermic,

TABLE 5: Calculated Energies ($D_{AB,s}$, in eV) for the Dissociation of CH_x Species ($x = 4, 3, 2, 1$) with the Involvement of Chemisorbed Oxygen on Metal Surface (s = Surface)

	Ni		Pd		Pt		Cu	
	top	hol	top	hol	top	hol	top	hol
$CH_{4,s} + O_s \rightarrow CH_{3,s} + OH_s$	−0.66	1.24	0.03	0.84	−0.12	0.31	−0.77	1.05
$CH_{3,s} + O_s \rightarrow CH_{2,s} + OH_s$	−0.51	1.39	0.14	0.95	−0.10	0.33	−1.22	0.60
$CH_{2,s} + O_s \rightarrow CH_s + OH_s$	−1.95	−0.05	−0.92	−0.11	−1.46	−1.03	−1.05	0.77
$CH_s + O_s \rightarrow C_s + OH_s$	−0.45	1.45	−0.53	0.28	−0.31	0.12	0.00	1.82
Δ[a]	−0.69	1.21	−0.68	0.13	−0.75	−0.32	−2.37	−0.55

[a] Difference between the dissociation energies with and without the involvement of chemisorbed oxygens.

TABLE 6: Calculated Combination (1) and Desorption (2) Energies[a] (eV) (g = Gas, s = Surface)

	Ni		Pd		Pt		Cu	
	(1)	(2)	(1)	(2)	(1)	(2)	(1)	(2)
$H_s + H_s \rightarrow H_{2,s} \rightarrow H_{2,g}$	1.09	0.03	0.46	0.00	0.37	−0.01	−0.52	−0.03
	1.29*		0.89*		0.83*		0.27*	
$C_s + O_s \rightarrow CO_s$[b] $\rightarrow CO_g$	−0.60	2.19	−2.52	1.46	−1.91	1.70	−3.06	0.01
	1.32*		0.01*		0.39*		0*,[c]	
$CO_g + O_s \rightarrow CO_{2,s} \rightarrow CO_{2,g}$	−0.87	0.00	−2.40	0.03	−2.25	−0.03	−1.41	−0.02
$H_s + O_s \rightarrow OH_s$	0.12		0.13		−0.32		−0.55	
$H_s + HO_s \rightarrow H_2O_s \rightarrow H_2O_g$	0.81	0.00	−1.36	0.00	−0.85	−0.02	−0.73	−0.02
$CH_{3,s} + CH_{3,s} \rightarrow C_2H_{6,g}$	0.36		−0.98		−0.52		−1.76	
$CH_{2,s} + CH_{2,s} \rightarrow C_2H_{4,g}$	1.21		−0.93		−0.51		−1.81	
$CH_s + CH_s \rightarrow C_2H_{2,g}$	3.62		0.82		2.76		−1.66	

[a] The molecular species H_2, CO, CO_2, and H_2O formed after combination are assumed to be terminally adsorbed with the molecular axis perpendicular to the metal surface. Values with asterisk are the calculated activation energies using eq 16. [b] CO is coordinated via C; it prefers the on-top site on Ni and Cu and the hollow site on Pd and Pt. [c] Negative values are obtained, and so they are set as zero.

but shows high activation energy. Semiempirical BOC-MP calculation gave similar high activation energy for the combination reaction on Ni.[12a] Since the activation energy E^*_{C+O} is large compared to those for the dehydrogenations ($CH_{x,s} \rightarrow CH_{x-1,s}$), it was inferred[12a] that the oxidation of the adsorbed C species on Ni is the rate-determining step. On Cu, the combination energy, C_{C+O}, is very negative. The $-C_{C+O}$ value is even larger than the "reduced" adsorption energy μ_E (2.15 eV) (see eq 16). Therefore, negative activation energy is obtained by using the BOC-MP formula.

The desorptions of CO_s on the transition metals are strongly endothermic. This means that after combination, CO can stick strongly to the surfaces. For M = Pd and Pt, the combination energies are low enough to compensate the desorption energies required. The desorption energy on the metal varies in the order of Ni > Pt > Pd. It is shown that CO is weakly adsorbed on Cu, similar to the H_2 case.

The reactions for the formation of CO_2 are all energetically favorable. So adsorbed O_s possesses a strong tendency to oxidize gas CO_g to CO_2. Therefore, the CO_2 selectivity would very much depend on the amount of adsorbed oxygen present on the surface. It was shown[13] that on an oxygen-rich surface, the selectivity of CO_2 was higher than that of CO and with the consumption of surface oxygen, CO selectivity increases while the CO_2 selectivity falls. In an oxygen-depleted environment, high selectivity of CO was obtained.[5c]

The formation of OH by the reaction $O_s + H_s \rightarrow OH_s$ is less favorable on Ni than on Pt, in agreement with the experimental observation.[6] The difference in H_2 selectivity between Ni and Pt was explained[6] by the relative instability of OH species on Ni surface which curtails the formation of H_2O. On the other hand, the calculated results show that the formation of H_2O is much less favorable on Ni than on Pt. This explains why Ni catalysts can give significantly higher H_2 selectivities than Pt catalysts in OMS experiments. According to the calculated results, Pd would be more selective to H_2O than Pt.

3.3.2. $CH_{x,s}$ Couplings. Since surface CH_x species are intermediates in the OMS reaction according to the methane pyrolysis mechanism, we here examined the energetics for the coupling processes of CH_x on the metal surfaces. In section 3.1.4 we showed that no abstraction of H from CH_x to produce gas-phase $CH_{x-1,g}$ is expected over the metal surfaces. However, one cannot exclude the possibility for the couplings of the surface species $CH_{x,s}$:

$$CH_{x,s} + CH_{x,s} \rightarrow C_2H_{2x,g} \; (x = 3, 2, 1) \qquad (17)$$

We have thus calculated the combination energies of eq 17. The results are given in the lower part of Table 6. On Ni, the combination reaction $CH_{3,s} + CH_{3,s} \rightarrow C_2H_6$ is mildly endothermic. On Pd and Pt, the situations are just the opposite. On the other hand, the formation of C_2H_6 is more favorable on Pd than on Pt. The combination $2CH_{2,s} \rightarrow C_2H_4$ is rather endothermic on Ni, but also exothermic on Pd and Pt. The combination $2CH_s \rightarrow C_2H_2$ is highly endothermic on Ni and Pt, but mildly endothermic on Pd. So the combination energies of $2CH_{x,s}$ on Pd are the least among the transition metals. In conclusion, Ni shows little ability to mediate the formation of higher carbon products. The combination reactions of $CH_{x,s}$ with $x = 3$ and 2 on Pd and Pt are energetically favorable and hence competes with the dissociation processes. Furthermore, the coupling reactions are more favorable on Pd than on Pt. In the OMS experiments of Tornianen and Schmidt[6] (at short contact time), C_2 production was up to 14% selectivity over Pd, 2.4−4.0% over Pt, and less than 0.1% over Ni. The trend in the calculated combination energies is in full agreement with the experimental observations.

In the case of Cu, the calculated combination energies are all rather negative. This means that if $CH_{x,s}$ species are generated on the surface, the formation of higher carbon products occurs readily.

4. Conclusions

Quasirelativistic density-functional calculations have been carried out to investigate the partial oxidation of methane to syngas (OMS) on transition and coinage metal M(111) surfaces (M = Ni, Pd, Pt, Cu). Ni_7, Pd_{10}, Pt_{10}, and Cu_{10} clusters were used to simulate the different metals. Adsorption energies of a series of intermediate species were determined, where the preferred sites were identified and the influence of cluster size on the calculated results was examined. On the basis of these results, as well as on the calculated bond strengths of the free species concerned, the dissociation energies of methane and combination energies for syngas and byproduct formations have been evaluated. Meanwhile, the simple analytic BOC-MP formula proposed by Shustorovich was used to estimate the activation energies. The steps for methane dissociation are also examined in the presence of chemisorption oxygen, which is assumed to participate in the OMS reaction. We arrive at the following major conclusions.

(1) To model the metal surfaces, the chosen clusters are sufficient to give qualitatively reliable results. The calculated adsorption energies are in reasonable agreement with available experimental data. The cluster size effect on the calculated reaction energies and activation energies is not significant. However, when different metals are compared, the cluster size effect has to be taken into account.

(2) The reaction of hydrogen-abstraction from CH_4 by the metals to produce gas-phase CH_3 is thermodynamically rather unfavorable. Therefore, the products formed do not correspond to $H_s + CH_{3,g}$, as in the case for metal oxides.

(3) The dissociation of methane is readily activated by the transition metals. The total dissociation energies calculated vary in the order of Ni < Pd ≈ Pt. This order corresponds to the experimental order in methane conversions on the transition metal catalysts (Ni > Pd ≈ Pt). Therefore, the difference in methane conversions for the metals can be understood by the comparison of the total dissociation energies on the metals. The total dissociation energy on Cu is calculated to be strongly endothermic and the activation energies for the discrete dehydrogenation steps are rather high. This is the reason why Cu catalysts do not mediate methane dissociation.

(4) The relativistic effects facilitate the methane dissociation and increase strongly from M = Ni to Pt. Without relativistic effects, the dissociation of methane on Pt would become difficult.

(5) The presence of oxygen located at metal on-top site (O^{top}) increases the adsorption energy of H, thereby promoting the methane dissociation steps on the metal surface. Oxygen at hollow site (O^{hol}) promotes methane dissociation on Pt and Cu, but is not beneficial to that on Ni and Pd. A general feature is that methane dissociation involving O^{top} has significantly lower dissociation energy than that involving O^{hol}. The M-O bond possesses strong covalent character, which might be one of the reasons for the different chemical reactivities of O^{top} and O^{hol} toward the dissociation of methane.

(6) The difference in the H_2 selectivities can be associated with the difference in the stabilities of OH on the metals.

(7) Gas-phase CO_g and adsorbed O_s can combine easily to form CO_2. Therefore, the selectivity of CO_2 will be dependent on the amount of adsorbed oxygen present on the surface. The conclusion is in concord with the experimental facts.

(8) The coupling reactions, viz. $CH_{x,s} + CH_{x,s} \rightarrow C_2H_{2x,g}$ with $x = 3$ and 2, on Pd and Pt are energetically favorable. These reactions will compete with the $CH_{x,s}$ dissociation reactions. The calculated trend in the combination energies is consistent with the observed experimental trend in C_2 selectivities over the Ni, Pd, and Pt metals.

We should point out that although all the conclusions are adequately supported by the data, some conclusions may be tentative because the OMS reactions at metal surfaces are complicated. For the present topics studied, an accurate evaluation of the adsorption energies for a number of intermediate species is a key step in order to "correctly" describe the thermodynamic trends. However, accurate determination of adsorption energies has been proven to be difficult. In high-level "ab initio" calculations, only a rather limited cluster size can be adopted to model a metal surface. Our results show about 0.5 eV uncertainty in the calculated adsorption energies. However, the model and level of theory used allow at least a semiquantitative discussion about the trends. This work could serve as a model for theoretical studies of complicated systems in surface chemistry.

Acknowledgment. We thank a referee for constructive comments. This work was supported by a Faculty Research Grant (FRG/94-95/II-53) of the Hong Kong Baptist University and by the Natural Science Foundation of Fujian Province, P. R. China.

References and Notes

(1) Prettre, M.; Eichner, C.; Perrin, M. *J. Chem. Soc., Faraday Trans.* **1946**, *43*, 335.

(2) (a) Vernon, P. D. F.; Green, M. L. H.; Cheetham, A. K.; Ashcroft, A. T. *Catal. Lett.* **1990**, *6*, 181. (b) Vernon, P. D. F.; Green, M. L. H.; Cheetham, A. K.; Ashcroft, A. T. *Catal. Today* **1992**, *13*, 417.

(3) Dissanayyake, D.; Rosynek, M. P.; Kharas, K. C. C.; Lunsford, J. H. *J. Catal.* **1991**, *132*, 117.

(4) (a) Boucouvalas, Y.; Zhang, Z. L.; Verykios, X. E. *Catal. Lett.* **1994**, *27*, 131. (b) Tsipouriari, V. A.; Efstathiou, A. M.; Zhang, Z. L.; Verykios, X. E. *Catal. Today* **1994**, *21*, 579. (c) Zhang, Z. L.; Verykios, X. E. *J. Chem. Soc., Chem. Commun.* **1995**, 71.

(5) (a) Hickman, D. A.; Schmidt, L. D. *J. Catal.* **1992**, *138*, 267. (b) Hickman, D. A.; Schmidt, L. D. *Science* **1993**, *259*, 343. (c) Hickman, D. A.; Haupfear, E. A.; Schmidt, L. D. *Catal. Lett.* **1993**, *17*, 223.

(6) (a) Torniainen, P. M.; Chu, X.; Schmidt, L. D. *J. Catal.* **1994**, *146*, 1. (b) Bharadwaj, S. S.; Schmidt, L. D. *J. Catal.* **1994**, *146*, 11.

(7) (a) Choudhary, V. R.; Rajput, A. M.; Prabhakar, B. *Catal. Lett.* **1992**, *15*, 363. (b) Choudhary, V. R.; Rajput, A. M.; Rane, V. H. *Catal. Lett.* **1992**, *16*, 269. (c) Choudhary, V. R.; Rajput, A. M.; Prabhakar, B. *J. Catal.* **1993**, *139*, 326. (d) Choudhary, V. R.; Rane, V. H.; Rajput, A. M. *Catal. Lett.* **1993**, *22*, 289.

(8) (a) Erdöhelyi, A.; Cserényi, J.; Solymosi, F. *J. Catal.* **1993**, *141*, 287. (b) Solymosi, F.; Erdöhelyi, A.; Cserényi, J. *Catal. Lett.* **1992**, *16*, 399.

(9) Mallens, E. P. J.; Hoebink, J. H. B. J.; Marin, G. B. *Catal. Lett.* **1995**, *33*, 291.

(10) (a) Buyevskaya, O. V.; Wolf, D.; Baerns, M. *Catal. Lett.* **1994**, *29*, 249. (b) Walter, K.; Buyevskaya, O. V.; Wolf, D.; Baerns, M. *Catal. Lett.* **1994**, *29*, 261.

(11) (a) Au, C. T.; Hu, Y. H.; Wan, H. L. *Catal. Lett.* **1994**, *27*, 199. (b) Au, C. T.; Hu, Y. H.; Wan, H. L. *Catal. Lett.* **1996**, *36*, 159. (c) Au, C. T.; Wang, H. Y.; Wan, H. L. *J. Catal.* **1996**, *158*, 343. (d) Wang, H. Y.; Au, C. T. *Catal. Lett.* **1996**, *38*, 77. (e) Au, C. T.; Wang, H. Y.; Wan, H. L. *Catal. Lett.* **1996**, *41*, 159. (f) Wang, H. Y.; Au, C. T.; Wan, H. L. *Chem. Res. Chin. Univ.* **1996**, *12*, 285.

(12) (a) Hu, Y. H.; Ruckenstein, E. *J. Catal.* **1996**, *158*, 260. (b) Hu, Y. H.; Ruckenstein, E. *Catal. Lett.* **1995**, *34*, 41. (c) Ruckenstein, E.; Hu, Y. H. *Catal. Lett.* **1995**, *35*, 265.

(13) Au, C. T.; Wang, H. Y. *J. Catal.* **1997**, *167*, 337.

(14) (a) Lee, M. B.; Yang, Q. Y.; Tang, S. L.; Ceyer, S. T. *J. Chem. Phys.* **1986**, *85*, 1693. (b) Lee, M. B.; Yang, Q. Y.; Ceyer, S. T. *J. Chem. Phys.* **1987**, *87*, 2724.

(15) Kaminsky, M. P.; Winograd, N.; Geoffroy, G. L. *J. Am. Chem. Soc.* **1986**, *108*, 1315.

(16) Campbell, R. A.; Szanyi, J.; Lenz, P.; Goodman, D. W. *Catal. Lett.* **1993**, *17*, 39.

(17) (a) Shustorovich, E. J. *J. Am. Chem. Soc.* **1984**, *106*, 6479. (b) Shustorovich, E. J.; Baetzold, R. C. *Science* **1985**, *227*, 876. (c) Shustorovich, E. J. *Acc. Chem. Res.* **1988**, *21*, 183. (d) Shustorovich, E. J. *Adv. Catal.* **1990**, *37*, 101.

(18) Upton, T. H. *J. Vac. Sci. Technol.* **1982**, *20*, 527.

(19) Anderson, A. B.; Maloney, J. J. *J. Phys. Chem.* **1988**, *92*, 809.
(20) (a) Schüle, J.; Siegbahn, P.; Wahlgren, U. *J. Chem. Phys.* **1988**, *89*, 6982. (b) Swang, O.; Faegri, K., Jr.; Gropen, O.; Wahlgren, U.; Siegbahn, P. *Chem. Phys.* **1991**, *156*, 379.
(21) (a) Yang, H.; Whitten, J. L. *J. Am. Chem. Soc.* **1991**, *113*, 6442. (b) Yang, H.; Whitten, J. L. *J. Chem. Phys.* **1992**, *96*, 5529.
(22) (a) Burghgraef, H.; Jansen, A. P. J.; van Santen, R. A. *Faraday Discuss.* **1993**, *96*, 337. (b) Burghgraef, H.; Jansen, A. P. J.; van Santen, R. A. *J. Chem. Phys.* **1994**, *101*, 11012.
(23) Jansen, A. P. J.; Burghgraef, H. *Surf. Sci.* **1995**, *344*, 149.
(24) Kratzer, P.; Hammer, B.; Nørskov, J. K. *J. Chem. Phys.* **1996**, *105*, 5595.
(25) (a) Anderson, A. B. *J. Am. Chem. Soc.* **1977**, *99*, 696. (b) Yu, J.; Anderson, A. B. *J. Am. Chem. Soc.* **1990**, *112*, 7218.
(26) Minot, C.; van Hove, M. A.; Somorjai, G. A. *Surf. Sci.* **1982**, *127*, 441.
(27) Zheng, C.; Apeloig, Y.; Hoffmann, R. *J. Am. Chem. Soc.* **1988**, *110*, 749.
(28) (a) Blomberg, M. R. A.; Brandemark, U.; Siegbahn, P. E. M. *J. Am. Chem. Soc.* **1983**, *105*, 5557. (b) Blomberg, M. R. A.; Siegbahn, P. E. M.; Nagashima, U.; Wennerberg, J. J. *Am. Chem. Soc.* **1991**, *113*, 424.
(29) Burghgraef, H.; Jansen, A. P. J.; van Santen, R. A. *J. Chem. Phys.* **1993**, *98*, 8810.
(30) ADF program package, version 2.0.1: (a) Baerends, E. J.; Ellis, D. E.; Ros, P. *Chem. Phys.* **1973**, *2*, 41. (b) te Velde, G.; Baerends, E. J. *J. Comp. Phys.* **1992**, *99*, 84.
(31) Vosko, S. H.; Wilk, L.; Nusair, M. *Can. J. Phys.* **1980**, *58*, 1200.
(32) Becke, A. D. *Phys. Rev.* **1988**, *A38*, 3098.
(33) Perdew, J. P. *Phys. Rev.* **1986**, *B33*, 8822.
(34) Ziegler, T.; Tschinke, V.; Baerends, E. J.; Snijders, J. G.; Ravenek, W. *J. Phys. Chem.* **1989**, *93*, 3050.
(35) Panas, I.; Schüle, J.; Siegbahn, P.; Wahlgren, U. *Chem. Phys. Lett.* **1988**, *149*, 265.
(36) Shustorovich, E. *Surf. Sci.* **1986**, *176*, L863.
(37) Bondi, A. *J. Phys. Chem.* **1964**, *68*, 441.
(38) Belgued, M.; Pareja, P.; Amariglio, A.; Amariglio, H. *Nature* **1991**, *352*, 789.
(39) Børve, K. J.; Pettersson, L. G. M. *J. Phys. Chem.* **1991**, *95*, 3214.
(40) Mehandru, S. P.; Anderson, A. B.; Brazdil, J. F. *J. Am. Chem. Soc.* **1988**, *110*, 1715.
(41) Stiakaki, M.-A. D.; Tsipis, A. C.; Tsipis, C. A.; Xanthopoulos, C. E. *J. Mol. Catal.* **1993**, *82*, 425.
(42) Driscoll, D. J.; Martir, W.; Wang, J.-X.; Lunsford, J. H. *J. Am. Chem. Soc.* **1985**, *107*, 58.
(43) Imbihl, R.; Demuth, J. E. *Surf. Sci.* **1986**, *173*, 395.
(44) Beckerle, J. D.; Yang, Q. Y.; Johnson, A. D.; Ceyer, S. T. *J. Chem. Phys.* **1987**, *86*, 7236.
(45) (a) Beebe, T. P., Jr.; Goodman, D. W.; Kay, B. D. *J. Chem. Phys.* **1987**, *87*, 2305. (b) Beebe, T. P., Jr.; Goodman, D. W.; Kay, B. D.; Yates, J. T., Jr. *J. Chem. Phys.* **1987**, *87*, 87.
(46) Christmann, K.; Schober, O.; Ertl, G.; Neumann, M. *J. Chem. Phys.* **1974**, *60*, 4528.